






# Cholinergic and hippocampal systems facilitate cross-domain cognitive recovery after stroke

 Michael J. O’Sullivan,<sup>1,2,†</sup> Lena K. L. Oestreich,<sup>1,3,†</sup>  Paul Wright<sup>4</sup> and  Andrew N. Clarkson<sup>5</sup>

<sup>†</sup>These authors contributed equally to this work.

See Geranmayeh (<https://doi.org/10.1093/brain/awac142>) for a scientific commentary on this article.

Spontaneous recovery of motor and cognitive function occurs in many individuals after stroke. The mechanisms are incompletely understood, but may involve neurotransmitter systems that support neural plasticity, networks that are involved in learning and regions of the brain that are able to flexibly adapt to demand (such as the ‘multiple-demand system’). Forty-two patients with first symptomatic ischaemic stroke were enrolled in a longitudinal cohort study of cognitive function after stroke. High-resolution volumetric, diffusion MRI and neuropsychological assessment were performed at a mean of  $70 \pm 18$  days after stroke. Cognitive assessment was repeated 1 year after stroke, using parallel test versions to avoid learning effects, and change scores were computed for long-term episodic, short-term and working memory. Structural MRI features that predicted change in cognitive scores were identified by a two-stage analysis: a discovery phase used whole-brain approaches in a hypothesis-free unbiased way; and an independent focused phase, where measurements were derived from regions identified in the discovery phase, using targeted volumetric measurements or tractography. Evaluation of the cholinergic basal forebrain, based on a validated atlas-based approach, was included given prior evidence of a role in neural plasticity.

The status of the fornix, cholinergic basal forebrain and a set of hippocampal subfields were found to predict improvement in long-term memory performance. In contrast to prior expectation, the same pattern was found for short-term and working memory, suggesting that these regions are part of a common infrastructure that supports recovery across cognitive domains. Associations between cholinergic basal forebrain volume and cognitive recovery were found primarily in subregions associated with the nucleus basalis of Meynert, suggesting that it is the cholinergic outflow to the neocortex that enables recovery. Support vector regression models derived from baseline measurements of fornix, cholinergic basal forebrain and hippocampal subfields were able to explain 62% of change in long-term episodic and 41% of change in working memory performance over the subsequent 9 months.

The results suggest that the cholinergic system and extended hippocampal network play key roles in cognitive recovery after stroke. Evaluation of these systems early after stroke may inform personalized therapeutic strategies to enhance recovery.

- 1 UQ Centre for Clinical Research and Institute of Molecular Bioscience, The University of Queensland, Brisbane, Australia
- 2 Department of Neurology, Royal Brisbane and Women’s Hospital, Brisbane, Australia
- 3 Centre for Advanced Imaging, The University of Queensland, Brisbane, Australia
- 4 Institute of Psychiatry, Psychology and Neuroscience, King’s College London, London, UK
- 5 Department of Anatomy, Brain Health Research Centre and Brain Research New Zealand, University of Otago, Dunedin 9011, New Zealand

Received September 25, 2021. Revised December 28, 2021. Accepted January 27, 2022. Advance access publication February 21, 2022

© The Author(s) 2022. Published by Oxford University Press on behalf of the Guarantors of Brain.

This is an Open Access article distributed under the terms of the Creative Commons Attribution-NonCommercial License (<https://creativecommons.org/licenses/by-nc/4.0/>), which permits non-commercial re-use, distribution, and reproduction in any medium, provided the original work is properly cited. For commercial re-use, please contact [journals.permissions@oup.com](mailto:journals.permissions@oup.com)

Correspondence to: Prof Michael J. O’Sullivan  
Office of Research & Implementation  
Building 34, Royal Brisbane and Women’s Hospital  
Butterfield St, Herston, 4029, QLD, Australia  
E-mail: m.osullivan1@uq.edu.au

**Keywords:** stroke; prognosis; neuroplasticity; hippocampus; memory

**Abbreviations:** AD = axial diffusivity; ChBF = cholinergic basal forebrain; DS = digit span; FA = fractional anisotropy; FCSRT = Free and Cued Selective Reminding Test; FW = free-water; MoCA = Montreal Cognitive Assessment; SVR = support vector regression; TBSS = tract-based spatial statistics

## Introduction

Spontaneous recovery of cognitive function occurs in many individuals in the months following brain injury.<sup>1</sup> Recovery occurs across multiple cognitive domains, including long-term episodic and working memory. Lesion mapping studies have suggested distinct associations between lesion location and working or episodic memory deficits after stroke.<sup>2</sup> A similar dissociation could apply to cognitive recovery, through domain and network-specific mechanisms of plasticity and neural adaptation. Generic mechanisms may also operate that support recovery across multiple domains. The latter might include neurotransmitter systems that support plasticity or systems that are able to support learning or cognition across multiple domains dependent on context. For example, the multiple-demand system of the brain<sup>3</sup> is increasingly engaged across a variety of cognitive tasks as task complexity, time pressure and associations with reward increase.<sup>4</sup> A role for cortical regions that are part of the multiple-demand system is suggested by functional MRI studies of recovery from aphasia.<sup>5</sup>

In the healthy brain, long-term episodic memory is supported by an extended hippocampal network that incorporates the hippocampus, fornix, diencephalon and retrosplenial cortex.<sup>6</sup> Working memory, on the other hand, is supported by a distinct network that includes regions in the frontal and parietal cortices.<sup>7</sup> These domain-specific anatomical networks are innervated by ascending neurotransmitter systems, such as the cholinergic, noradrenergic and serotonergic systems, which project widely to subcortical and cortical regions. Interactions between these systems appear to be critical to performance. Working memory, for example, is supported by a complex interplay between cholinergic inputs and neural oscillations across a large-scale cortical network.<sup>8</sup> The interplay between specific functional networks and ascending systems also appears to be critical for outcome after injury. In experimental lesion studies in the macaque, the effect of fornix transection on long-term memory is much more severe if preceded by cholinergic denervation.<sup>9</sup> Consistent with this finding, in a previous neuroimaging study in humans, we demonstrated that higher grey matter volumes in the cholinergic basal forebrain (ChBF) enabled greater neural adaptation through a redistribution of cognitive load to tracts other than the fornix in individuals with early fornix degeneration.<sup>10</sup> Cholinergic innervation is essential for driving skilled motor learning after brain injury.<sup>11,12</sup> Ascending neurotransmitter systems may therefore provide a common machinery to support recovery of function after injury. However, the exact role that cholinergic signalling pathways play, and the importance of interactions with specific cortical regions, remains to be elucidated.

The objective of this study was to identify systems that enable spontaneous recovery after focal brain injury. To achieve this, long-

term episodic, short-term and working memory change were measured in a cohort of individuals that had suffered a first ischaemic stroke. Detailed structural MRI was performed approximately 3 months after stroke and change in cognition was then assessed over the succeeding 9 months (to a point 1 year after stroke). Associations with change were tested in non-lesioned grey and white matter, and specifically in the ChBF using a focused region of interest approach.<sup>13</sup> Diffusion tractography and measurements of grey matter volume in atlas-defined subregions were performed as guided by the results of the whole brain analysis and previous findings reported in the literature. The prediction was that ChBF structure would be associated with recovery across multiple domains but that other grey and white matter regions involved in recovery would show domain-specificity for either long-term episodic, short-term or working memory, consistent with the segregated networks supporting these distinct domains. Identifying the regions associated with recovery is important given the potential for neuromodulatory therapies to be applied to these regions.

## Materials and methods

### Participants

Patients with first symptomatic ischaemic stroke ( $n = 179$ ) were enrolled into a large study on cognitive outcome after stroke (STRATEGIC, NCT03982147) within 7 days of stroke. Data presented in this manuscript included a subset of 51 patients who additionally underwent research MRI and 12-month follow-up assessment of memory performance. Inclusion criteria were age over 50 years and stroke confirmed by neuroimaging (CT or MRI). Exclusion criteria were previous large-artery infarct, prior moderate to severe head injury, dementia or cognitive disorder or other established neurological disease, inability to converse fluently in English, active malignancy and inability to consent. Dysphasia or visual impairment severe enough to prevent a participant from providing informed consent or complete written cognitive tests were also exclusion criteria. This was based on clinical diagnosis of aphasia by either a treating speech and language therapist or the recruiting investigator (M.O.S.). The study protocol was approved by the London and Bromley Research Ethics Committee and the University of Queensland Research Ethics Committee. All participants gave written informed consent. Cognitive testing and research MRI were performed at approximately 3 months [days since stroke: mean = 69.61, standard deviation (SD) = 17.92] and follow-up clinical and cognitive evaluation at 12 months (days since stroke: mean = 386.95, SD = 33.08) after stroke.

## Clinical evaluation and stroke subtypes

All participants underwent comprehensive clinical evaluation including ascertainment of cardiovascular risk factor status and stroke subtyping investigations including neuroimaging, imaging of cervical arteries (CT angiography of Doppler ultrasound) and assessment of cardiac rhythm and structure. Smoking, diabetes mellitus, family history of stroke and/or cardiac disease and hypertension were assessed via self-report. Hypertension was defined as a diagnosis of high blood pressure or prescription of antihypertensive drugs. Ischaemic heart disease was defined as a history of acute coronary syndrome or a coronary artery intervention. Carotid stenosis was defined as >50% vessel narrowing identified on CT angiography or Doppler ultrasound. Atrial fibrillation was defined as AF on admission or other inpatient 12-lead ECG or sustained atrial fibrillation (>7 min) on subsequent prolonged Holter recordings. Cerebral small-vessel disease was defined by the presence of confluent or near-confluent MRI T<sub>2</sub>-weighted hyperintensity (corresponding to grade 2 or 3 according to Fazekas et al.<sup>14</sup>) in either deep or periventricular white matter.

Clinical MRI was used to classify infarcts by hemisphere and arterial territory: cortical lesions were classified into anterior, middle and posterior cerebral artery territories. Middle cerebral artery infarcts were furthermore subclassified into middle–anterior, middle–posterior and middle striatocapsular lesions. Lesions in the thalamus were classified as thalamic infarcts and other lesions in white or deep grey matter with a diameter of less than 15 mm were classified as non-thalamic lacunar lesions. The characteristics of the sample in terms of stroke location, subtype, demographics and risk factor status are summarized in Table 1.

## Cognitive tests and measures

General cognitive ability was measured with the Montreal Cognitive Assessment (MoCA), a short test assessing performance across multiple cognitive domains (attention, executive function, orientation, language, abstract reasoning and memory).<sup>15</sup> Long-term episodic memory was tested with the Free and Cued Selective Reminding Task (FCSRT).<sup>16</sup> In this test, participants are instructed to learn 16

items presented four at a time on a card placed in front of them. They are asked to point to, and name, each item (e.g. grapes) linked to a category cue (e.g. fruit). After a 20-s interference period, participants are given 2 min to recall as many items as possible (delayed free recall). Cued recall of items that are not retrieved by initial free recall is then tested by presenting the category cues. If an item is not retrieved within 10 s, the participant is reminded of the item. Delayed Free Recall and Total Recall (free recall plus cued recall) are the main measures of performance.<sup>16</sup> Short-term and working memory were evaluated with digit span (DS).<sup>17</sup> Participants are read a sequence of numbers and asked to repeat the sequence back to the examiner in the same order (DS forward), which is considered a measure of short-term memory. Alternatively, participants are asked to recall the sequence backwards, which involves mental manipulation of the number sequence and is therefore a measure of working memory. The sequences are increased in difficulty by one digit at a time until the participant is unable to remember the complete sequence, or until they repeated it incorrectly on two consecutive trials. The final score is the maximum sequence length successfully recalled.

The MoCA, FCSRT and DS tests were administered again at the 1-year follow-up assessment. For all three tests, alternative parallel versions were administered at follow-up to avoid learning effects from the first administration. The order of administration was counter-balanced, i.e. approximately half of the participants were tested with version A then version B, and approximately half version B then version A for each of the three tests.

Memory outcome scores were calculated by subtracting scores at 12 months from scores at the 3-month assessment, generating the following change scores:  $\Delta$ FCSRT delayed free recall;  $\Delta$ FCSRT total recall;  $\Delta$ DS forward; and  $\Delta$ DS backward.

Positive scores indicated memory improvement, negative scores worsening of memory performance and a score of zero reflected equivalent performance at both time points. Difference scores were used in all analyses below. Two participants did not complete FCSRT on follow-up. All analyses with FCSRT were therefore performed with 40 participants.

## Research MRI data acquisition

Research MRI scans were collected on a 3 T MR750 MR scanner (GE Healthcare). T<sub>1</sub>-weighted images were acquired with the MPRAGE sequence<sup>18</sup> using the following parameters: repetition time (TR) = 7.31 ms, echo time (TE) = 3.02 ms and flip angle = 11°. Images were acquired in the sagittal plane with field of view (FOV) = 270 × 270 mm, matrix size = 256 × 256 voxels and slice thickness and gap = 1.2 mm. T<sub>2</sub>-weighted fluid-attenuated inversion recovery (FLAIR) and fast recovery fast spin echo (FRFSE) sequences were acquired for lesion delineation. The FLAIR sequence was acquired with TR = 8000 ms, TE = 120–130 ms and flip angle = 90–111°. The FRFSE sequence was performed with TR = 4380 ms, TE = 54–65 ms and flip angle = 90–111°. Images were acquired in the axial plane with FOV = 240 × 240 mm for both sequences. The matrix size for the FLAIR sequence was 256 × 128 voxels and 320 × 256 voxels for the FRFSE sequence. Slice positions were aligned for both sequences with 36 slices at 4 mm thickness for FLAIR and 72 slices at 2 mm thickness for FRFSE.

Diffusion-weighted images were acquired with an echo planar imaging sequence with double refocused spin echo for 60 diffusion-sensitization directions at  $b = 1500$  s/mm<sup>2</sup> and six acquisitions without diffusion sensitization ( $b = 0$ ). Image geometry for the diffusion-weighted images covered the whole brain using 2 mm axial slices with matrix size of 128 × 128 voxels and FOV of 256 ×

**Table 1** Lesion characteristics and risk factors

Variable	Category/mean (SD)
<b>Lesion characteristics</b>	
Hemisphere (left/right)	23/19
Arterial territory (ACA/MCA <sub>ant</sub> /MCA <sub>pos</sub> /MCA <sub>str</sub> /PCA/lacunar/thalamic)	0/8/9/8/9/5/3
Volume (ml)	7761.07 (11865.61)
Fazekas (1/2/3)	20/18/4
<b>Risk factors</b>	
Carotid stenosis (yes/no)	5/37
Atrial fibrillation (yes/no/unknown)	9/30/3
Smoking (yes/no/previously)	5/24/13
Hypertension (yes <sup>a</sup> /yes <sup>b</sup> /no)	23/2/17
Diabetes mellitus, type 2 (yes <sup>a</sup> /yes <sup>c</sup> /yes <sup>d</sup> /no)	5/1/1/35
Ischaemic heart disease (yes/no)	8/34
Small-vessel disease (yes/no)	14/28
Family history (yes <sup>e</sup> /yes <sup>f</sup> /yes <sup>g</sup> /no)	10/16/5/11

ACA = anterior cerebral artery; MCA<sub>ant</sub> = middle cerebral artery, anterior; MCA<sub>pos</sub> = middle cerebral artery, posterior; MCA<sub>str</sub> = middle cerebral artery, striatocapsular; PCA = posterior cerebral artery. Fazekas: 1 = 'caps' or pencil-thin lining, 2 = smooth 'halo', 3 = irregular periventricular signal extending into the deep white matter.

<sup>a</sup>Controlled by medication; <sup>b</sup>uncontrolled; <sup>c</sup>controlled by diet; <sup>d</sup>controlled by insulin; <sup>e</sup>stroke; <sup>f</sup>cardiac disease; <sup>g</sup>stroke and cardiac disease.

256 mm, resulting in 2 mm isotropic resolution. Slices were aligned such that the intercommissural line was as close to the axial plane as possible. Acquisition was peripherally gated to the cardiac cycle, giving a sequence duration of 11–20 min, a TR of 10 000–14 118 ms and a TE of 66–78 ms with a flip angle of 90°.

## MRI preprocessing

Lesions were manually drawn on FLAIR images and, when necessary, confirmed on diffusion images acquired acutely. Lesion maps were co-registered into Montreal Neurological Institute (MNI) standard space, so that anatomically homologous brain areas were aligned. A study-specific lesion map was generated by combining all lesions in MNI space into a binary mask image (Supplementary Fig. 1).

Registration and segmentation of  $T_1$ -weighted images were performed using DARTEL,<sup>19</sup> an algorithm for diffeomorphic image registration implemented in SPM12 (Statistical Parametric Mapping software: <http://www.fil.ion.ucl.ac.uk/spm/>) run in MATLAB 2020a ([https://au.mathworks.com/products/new\\_products/release2020a.html](https://au.mathworks.com/products/new_products/release2020a.html)) Individual images were displayed in SPM12 to verify they were free from gross anatomical abnormalities. To reduce scanner-specific bias and improve registration,  $T_1$  images were semi-automatically centred at the anterior commissure and reoriented according to the anterior–posterior commissure line. Images were segmented into grey matter, white matter and CSF using the *New Segment* procedure. DARTEL was used to spatially normalize and modulate the segmented images.<sup>19</sup> The image intensity of each voxel was modulated by Jacobian determinants derived from spatial normalization to ensure that regional differences in the total amount of grey matter volume were conserved. The registered images were then transformed to MNI space. The normalized, modulated grey matter images were smoothed with an 8-mm full-width at half-maximum Gaussian kernel to increase the signal-to-noise ratio. Total intracranial volume was calculated by summing total grey matter, white matter and CSF. Absolute threshold masking of 0.1 was used to exclude voxels with a grey matter probability below 0.1 to avoid overlap around the borders between grey and white matter as well as grey matter and CSF.

Diffusion-weighted image data were preprocessed in Explore DTI v4.8.5.<sup>20</sup> Data were corrected for motion artefacts and eddy current distortions with reorientation of the gradient encoding vectors. Free-water (FW) imaging was used to remove partial volume effects induced by CSF contamination and to quantify the amount of extracellular FW by separating the diffusion properties of brain tissue from the surrounding extracellular FW.<sup>21</sup> The resulting FW-corrected diffusion-weighted image maps were then used to generate tensor images. Tissue-specific fractional anisotropy ( $FA_T$ ), axial diffusivity ( $AD_T$ ) and radial diffusivity ( $RD_T$ ) maps were generated from the FW-corrected tensor maps using *fslmaths*, a command line utility implemented in FSL.<sup>22</sup>

Whole-brain tractograms were generated in all participants using the constrained spherical deconvolution algorithm<sup>23</sup> with recursive calibration of the response function.<sup>24</sup> The tracking algorithm was set to terminate when the fibre orientation density amplitude fell below 0.1, the turning angle exceeded 45°, the path length was shorter than 50 mm or exceeded 500 mm.

## Design of analysis

The analysis was performed in two stages, a discovery phase (hypothesis-free) and a second hypothesis-driven validation phase (Fig. 1). Both phases tested associations with grey matter structure

and white matter microstructure separately. In the first phase, well-established whole-brain hypothesis-free approaches were adopted, namely voxel-based morphometry for grey matter and tract-based spatial statistics (TBSS) for white matter. The plan for the validation phase was to: (i) investigate grey matter regions in more detail using atlas-based labelling approaches to derive measurements of specific grey matter regions at a smaller scale and with higher anatomical specificity (implemented in FreeSurfer); and (ii) to use tractography to reconstruct fibre pathways implicated by TBSS and previous research and thereby to derive tract-specific measures of microstructure. In addition, we planned *a priori* to investigate associations with grey matter volume within the cholinergic basal forebrain, based on previous evidence of involvement of the cholinergic system in neural plasticity and adaptation to injury.<sup>9,10</sup>

## Hypothesis-free whole-brain analysis

To investigate associations with grey matter, four multiple linear regression voxel-based morphometry analyses were performed in SPM12 to test for associations between grey matter volume and memory outcome ( $\Delta$ FCSRT delayed free recall/ $\Delta$ FCSRT total recall/ $\Delta$ DS forward/ $\Delta$ DS backward). The study-specific lesion map was used as an exclusion mask to remove voxels containing lesions in one or more participants. Statistical thresholds were set to a familywise error corrected  $P \leq 0.05$  at cluster-level.

For white matter microstructure, Advanced Normalization Tools<sup>25</sup> TBSS (ANTs-TBSS) was used instead of the traditional FSL TBSS pipeline, as it has been shown to improve sensitivity and specificity of voxel-wise comparisons through improved registration algorithms.<sup>26</sup> ANTs-TBSS generates a study-specific template from  $T_1$ -weighted images in native space, which is preferable over registration to standard templates or most representative subjects as used in FSL TBSS.<sup>27</sup> This is particularly the case in clinical populations. Registration steps were carried out with ANTs v2.3.5.<sup>28</sup> In a first step, unweighted, averaged diffusion images (b0s) were non-linearly registered to native, bias-corrected and skull-stripped  $T_1$  images. In a second step, groupwise registration of  $T_1$  images was performed with four iterations of rigid, affine and non-linear symmetric image normalization registration.<sup>29</sup> The algorithm performs symmetric pair-wise mapping whereby an image is mapped onto a shape-based mean target generated from all input  $T_1$  images, which is then mapped back onto the individual  $T_1$  image. The final template has the same resolution as the original inputs. In a third step, the individual transforms generated during registration of native b0s to native  $T_1$  and native  $T_1$  to  $T_1$  group template are then used to warp metric maps (i.e. native  $FA_T/AD_T/RD_T/FW$ ) to the group template space. A binary white matter mask was created by thresholding the mean  $FA_T$  image to only contain voxels with  $FA_T < 0.2$ . Voxel-wise changes of white matter measurements ( $FA_T/AD_T/RD_T/FW$ ) associated with memory outcome ( $\Delta$ FCSRT delayed free recall/ $\Delta$ FCSRT total recall/ $\Delta$ DS forward/ $\Delta$ DS backward) were tested with four regression analyses (one per white matter metric) using non-parametric permutation tests (Randomize, FSL). Threshold-free cluster enhancement was used to avoid selecting an arbitrary cluster threshold. Data were tested against an empirical null distribution computed by 5000 permutations for each contrast, therefore generating statistical maps that are fully corrected for multiple comparisons across space. The significance level was set to a FWE corrected  $P \leq 0.05$ . To compute the proportion of white matter tracts included in a given

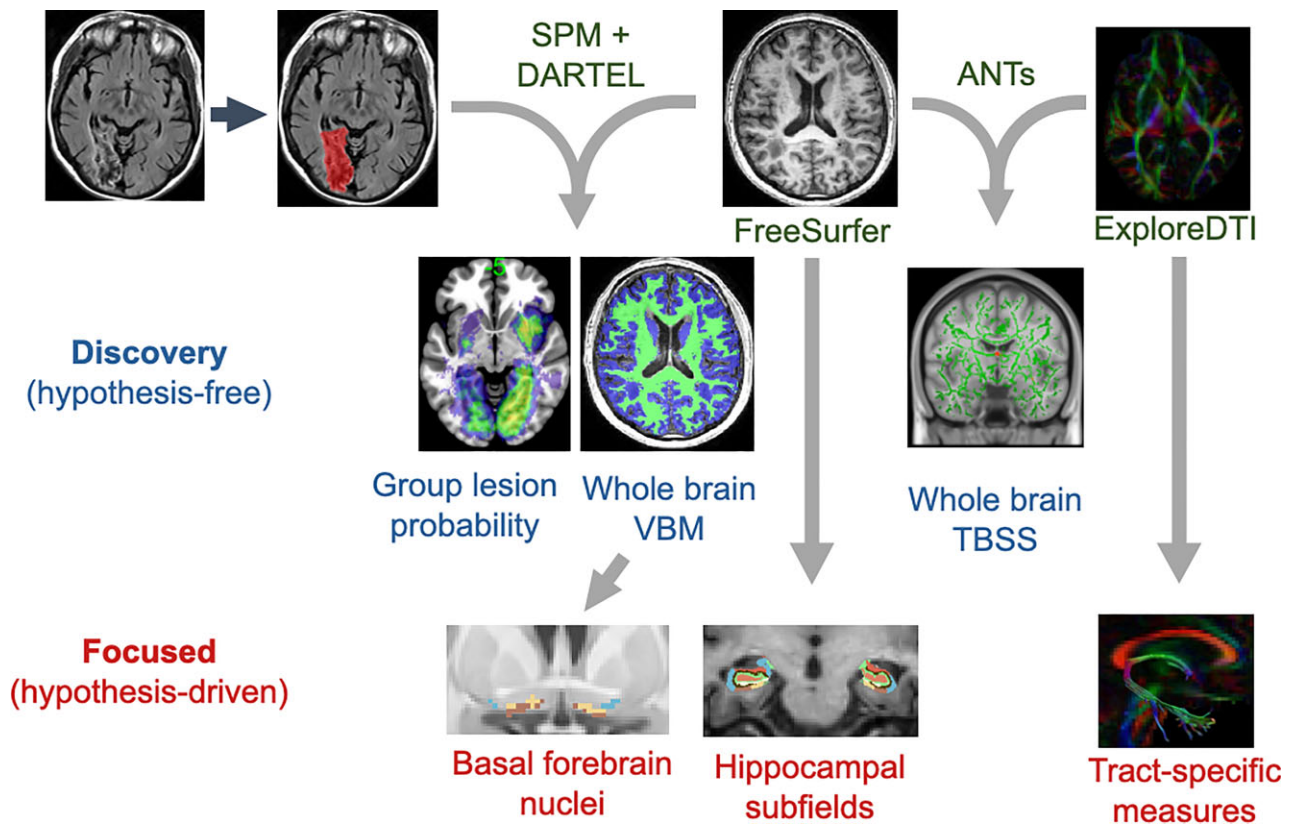


Figure 1 Analysis pipeline.

cluster, significant cluster maps were binarized and overlaid on the JHU DTI-based white-matter atlas.<sup>30</sup> Percentages of overlap with atlas-defined white matter tracts were then calculated using the *atlasquery* tool implemented in FSL.<sup>22</sup> Only white matter tracts that were reliably identified across regression analyses and contributed to memory outcome with the majority of their corresponding voxels, defined as >50% overlap with their respective atlas regions, were investigated further with tractography. Statistical maps plotting the corrected *P*-values were visualized using FSL (*TBSS-fill* and *FSLeyes*).

### Focused analysis

Hippocampal subfields were automatically segmented using a Bayesian statistical model with Markov random field priors to estimate labels from an *ex vivo* atlas of hippocampal subfields.<sup>31</sup> Hippocampal subfields were segmented by appending the flag *hippocampal-subfields-T1* to the *recon-all* command for processing *T*<sub>1</sub>-weighted images in FreeSurfer (v6.0, <http://surfer.nmr.mgh.harvard.edu/>).<sup>32</sup> Hippocampi were automatically segmented into 12 subfields: hippocampal tail, parasubiculum, presubiculum, subiculum, cornu ammonis (CA)1, CA3, CA4, hippocampus–amygdala transition area, granule cell and molecular layers of the dentate gyrus, molecular layer, fimbria and hippocampal fissure (Supplementary Fig. 2). Segmentations were checked visually for agreement with known hippocampal anatomy. Volumetric measurements were normalized according to total intracranial volume. Volumes calculated for each hippocampal segment were averaged across hemispheres.

Grey matter volume within the ChBF was measured using template regions that have been histologically validated against post-

mortem anatomy.<sup>13</sup> The MNI-registered ChBF map was applied to the normalized, modulated, grey-matter threshold masked and re-registered subject scans. ChBF volumes were calculated from all voxels within the mask, again applying normalization by total intracranial volume. The ChBF consists of several subregions with somatotopically organized projections to the cortex and subcortex (Supplementary Fig. 2). We therefore also tested associations between ChBF volume and memory outcome with a voxel-wise regression analysis in SPM12 confined to the ChBF mask (cluster-level FWE correction:  $P \leq 0.05$ ).

Tractography was performed using regions of interest as waypoints to extract tract reconstructions from whole-brain tractograms. The algorithm used to extract the fornix has been described in previous publications, including an earlier methodological study. Briefly, the fornix was delineated by placing a seed region of interest in a coronal plane to enclose the columns of the fornix at their inferior curve. An inclusion region of interest was drawn in the axial plane around the crus of the fornix at the inferior edge of the corpus callosum. Exclusion regions of interest were placed in anterior, posterior, superior and inferior planes at the limits of the fornix and to remove outlier tracts. In a subsample of participants from this study ( $n = 10$ ), tractography was performed by two raters to test reproducibility. Inter-rater intra-class correlations were  $\geq 0.82$ , indicating good inter-rater reproducibility.

### Statistical analysis

Change in memory performance was evaluated with paired sample *t*-tests between scores at 3- and 12-month assessments for FCSRT delayed free recall, FCSRT total recall, DS forward and DS backward. Improved and declined memory performance were defined as

increased and decreased scores at 12 months relative to 3 months, respectively. Participants with the same score at 3- and 12-month assessments were classified to exhibit stable memory performance.

Age, sex and baseline cognitive performance (MoCA score) collected at 3 months were included as covariates in all of the following analyses. Baseline scores on FCSRT and DS were added as covariates to analysis of their corresponding change scores to assess change in cognitive scores independently of initial memory performance. All analyses were repeated with risk factors (Table 1) as covariates. Due to the high number of covariates and relatively small sample size, these results are only reported if they differ from results without covarying for risk factors. For whole-brain voxel-based analyses, type I error was controlled using established approaches for each methodology with a whole-brain (familywise error corrected) significance level of  $P < 0.05$  (as described above for each specific analysis). For analysis of specific networks and structures, linear associations of memory outcome ( $\Delta$ FCSRT delayed free recall/ $\Delta$ FCSRT total recall/ $\Delta$ DS forward/ $\Delta$ DS backward) and microstructural or volumetric measurements were assessed using partial correlation coefficients, correcting for age, sex, baseline cognitive performance (MoCA) and baseline memory performance (FCSRT or DS). We performed multiple comparisons across recurrent measures and correlated measures that are not independent. In this circumstance, the Bonferroni correction is unduly conservative. We therefore used the FDR at a stringent level of 1% (0.01) and a more lenient level of 5% (0.05) to correct for multiple comparisons.

To estimate the overall explanatory power of the regions identified in the analyses, we investigated the extent to which fornix microstructure, ChBF and hippocampal subfield volumes collectively predicted memory outcome by performing four Support Vector Machine Regression (SVR) in MATLAB 2020a for each cognitive change score. We chose SVR over multiple regression analysis due to the large number of predictors as, relative to multiple regression, SVR is less prone to overfitting through the use of regularization. Individual participants were allocated randomly to either training (75%) or test (25%) sets. To further control for false positive inflation (type I error), 10 permutations per SVR were used. The generalizability of the SVRs were assessed by calculating the loss (mean squared error) for each cross-validated regression model. The function `fitrsvm` was used to fit a SVR model using standardized data and either a linear or Gaussian kernel in the training set. The generated model was used to predict responses in the test set.  $R^2$  was calculated to estimate how well the model generated

from the training set predicted the data in the test set. (Further detail on the SVR procedures is provided in the [Supplementary material](#)) To investigate whether memory outcome could instead be predicted from lesions, additional SVRs were performed with lesion characteristics (Table 1) as predictor variables and cognitive change scores as outcome variables.

## Data availability

Data included in the manuscript are available for sharing. Requests should be made to the corresponding author and will be considered by the investigators against the data sharing arrangements articulated in the protocol and ethical approval of the study.

## Results

Nine patients did not complete follow-up assessments: one died; two were excluded due to recurrent stroke; and six declined or did not respond to the invitation. The final patient sample ( $n = 42$ ) ranged in age from 53 to 86 years (mean = 70.76, SD = 8.03), completed a minimum of 9 and a maximum of 21 years of education (mean = 14.12, SD = 3.9), 29% ( $n = 12$ ) were female and 97.6% ( $n = 41$ ) were right-handed.

## Cognitive prognosis

Overall cognitive performance as measured by the MoCA remained relatively stable from 3 months (mean = 25.46, SD = 3.33) to 12 months (mean = 25.78, SD = 3.59) post-stroke. Based on a cut-off score of 26 (out of 30) on the MoCA,<sup>15</sup> 59% ( $n = 25$ ) of patients scored within the normal cognitive range and 41% ( $n = 17$ ) within the range of scores indicating mild cognitive impairment. Memory performance across the whole sample improved from baseline to follow-up assessments as indexed by FCSRT delayed free recall [ $t(39) = 2.09$ ,  $P = 0.043$ ], DS forward [ $t(41) = 5.91$ ,  $P < 0.001$ ] and DS backward [ $t(41) = 6.48$ ,  $P < 0.001$ ], but not FCSRT total recall (Fig. 2). Performance on FCSRT delayed recall improved in 72.5% and worsened in 27.5% of participants ( $\Delta$ FCSRT delayed free recall: mean = 2.23, SD = 6.74, IQR = -1.75–6.75). FCSRT total recall improved in 47.5%, remained stable in 25% and worsened in 27.5% of participants ( $\Delta$ FCSRT total recall: mean = 0.78, SD = 3.43, IQR = -1.0–3.0). DS improved in 76.2%, remained stable in 19% and deteriorated in 4.8% (DS forward: mean = 1.52, SD = 1.67, IQR = 0.75–3.0) and working memory (DS backwards) improved in 78.6%, remained

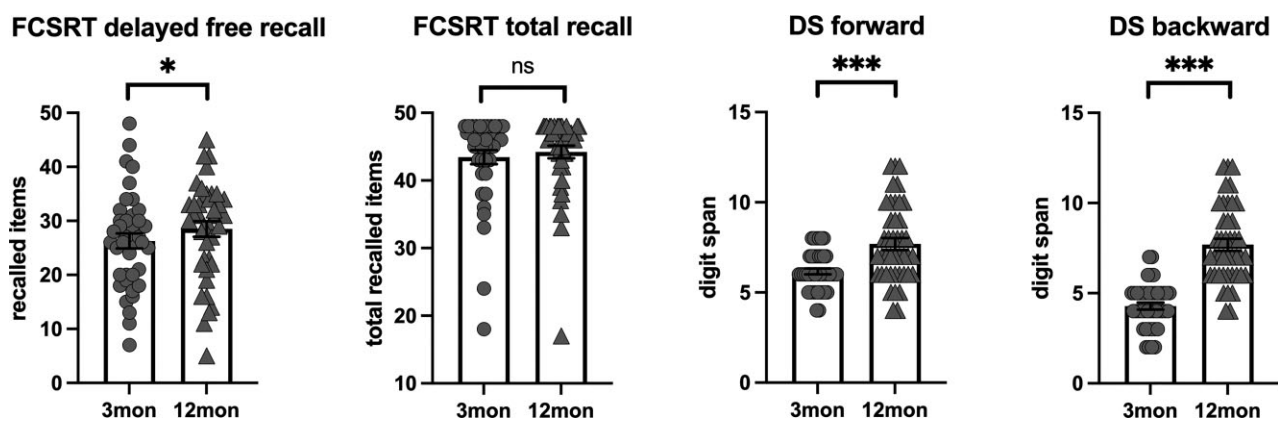
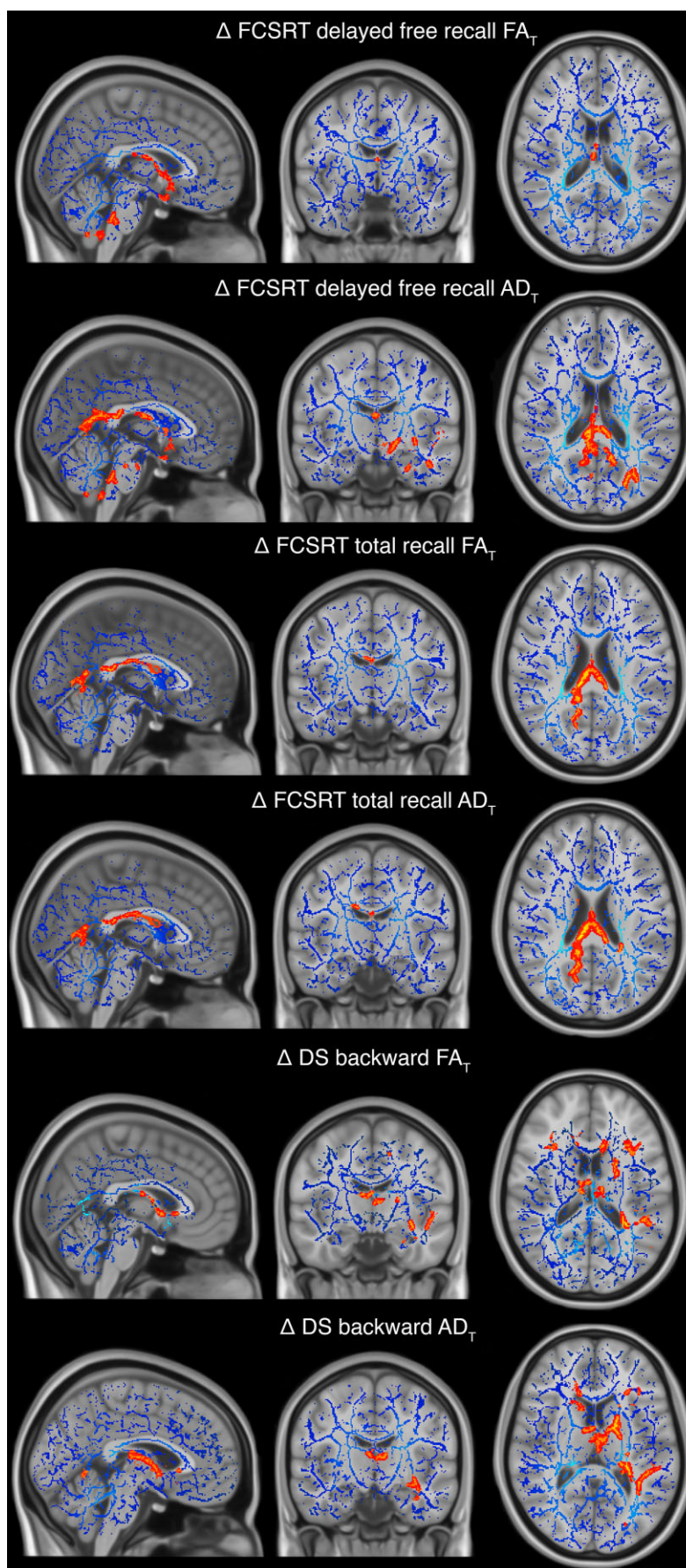


Figure 2 Cognitive prognosis. Memory performance at 3 months (circles) and 12 months (triangles) post-stroke. ns = not significant; error bars represent the standard error of the mean; \* $P \leq 0.05$ ; \*\* $P \leq 0.01$ ; \*\*\* $P \leq 0.001$ .



**Figure 3 TBSS results.** Increased tissue-specific fractional anisotropy (FA<sub>T</sub>) and axial diffusivity (AD<sub>T</sub>) were observed with memory improvement on FCSRT delayed free recall and total recall, as well as DS backward.

unchanged in 9.5% and deteriorated in 11.9% (DS backward: mean = 1.81, SD = 1.81, IQR = 1.0–3.0) of patients.

### Hypothesis-free whole-brain analyses

Positive associations were found between tissue microstructure and improved performance for FCSRT delayed free recall and FCSRT total recall. Significant positive associations were found within the body and column of the fornix for both recall measures and both microstructural metrics (FA<sub>T</sub> and AD<sub>T</sub>,  $P < 0.05$ , FWE-corrected; Fig. 3 and Table 2). Voxel-based morphometry demonstrated no associations between grey matter volume and change in long-term episodic memory performance that were significant at the whole-brain level.

Positive associations were also found between tissue microstructure and improved working memory performance (DS backwards). Significant positive associations were found within the body and columns of the fornix. There was substantial anatomical overlap in the regions associated with long-term episodic memory and working memory (Fig. 3 and Table 2). Furthermore, the peak of

the main FA<sub>T</sub> clusters (FCSRT delayed free recall/FCSRT total recall/DS backward) and two of the AD<sub>T</sub> clusters (FCSRT total recall/DS backward) were located in the body and column of the fornix. Voxel-based morphometry demonstrated no associations between grey matter volume and change in working memory performance that were significant at the whole-brain level.

### Focused analysis of specific networks

In line with previous research findings, the results of the whole brain TBSS analysis reliably identified large portions of the fornix (60.1–78.9%) to be associated with memory outcome across all regression analyses, which was therefore selected as a white matter pathway for further interrogation by tractography. Given the intimate anatomical association between the fornix and hippocampus,<sup>33</sup> volumetric measurements of hippocampal subfields were also performed and based on the *a priori* analysis plan, the ChBF was also assessed as a region of interest. Table 3 shows the partial (controlling for age, sex, MoCA baseline scores and baseline memory performance) correlation coefficients for change of cognition in

Table 2 ANTs-TBSS regression analysis with FCSRT and DS

Modality	Direction	Cluster size	Anatomical regions	Peak t-statistic	Peak MNI coordinates
<b>ΔFCSRT delayed free recall</b>					
FA <sub>T</sub>	Positive	31 948	Fornix (body and column: 78.9%) (peak) CC (splenium) (29.6%); corticospinal tract (lh: 3.3%; rh: 14.8%); ILF (lh: 10.1%); hippocampal cingulum (lh: 29.6%; rh: 7.6%); fornix (cres)/stria terminalis (lh: 24.7%; rh: 14.8%); SLF (rh: 11.8%); IOFF (lh: 8.4%; rh: 8.4%); UF (lh: 4.3%; rh: 4.1%); anterior cingulum (lh: 4.5%)	4.52	1, 3, 5
AD <sub>T</sub>	Positive	26 330	CC (splenium) (peak) (23.1%) Fornix (body and column: 60.1%); ATR (lh: 23.3%; rh: 29.4%); corticospinal tract (lh: 21.6%; rh: 20.1%); fornix (cres)/stria terminalis (lh: 29%); hippocampal cingulum (lh: 27.4%; rh: 7.5%); posterior cingulum (lh: 10%; rh: 1.6%); SLF (lh: 16.3%; rh: <0.1%); IOFF (rh: 16.1%); UF (lh: 4.2%); ILF (rh: 7.1%); forceps major (8.3%)	4.02	0, -33, 15
<b>ΔFCSRT total recall</b>					
FA <sub>T</sub>	Positive	9106	Fornix (body and column: 77.3%) (peak) CC (genu: 28%); ATR (lh: 21.5%; rh: 27.8%); anterior cingulum (lh: 8.3%; rh: 23.7%)	4.37	0, -1, 11
	Positive	7588	PLIC (rh: 29.2%) (peak) ATR (rh: 15.3%); fornix (cres)/stria terminalis (rh: 32.8%); external capsule (lh: 7.3%; rh: 9.1%); posterior corona radiata (rh: 15.2%); ILF (rh: 8.5%); IOFF (rh: 7.3%); SLF (rh: 4%)	4.28	28, -36, 16
AD <sub>T</sub>	Positive	17 036	Fornix (cres)/stria terminalis (rh: 61.6%) (peak) SLF (rh: 8.3%); PLIC (rh: 5.9%); corticospinal tract (lh: 7.3%; rh: 5.8%); ILF (rh: 7%); external capsule (rh: 3.4%); IOFF (rh: 15.8%)	3.91	32, -22, -8
	Positive	10 805	Fornix (body and column: 66.7%) (peak) ATR (lh: 23.7%; rh: 14.9%); UF (lh: 0.3%; rh: 1%); ALIC (lh: 7.3%; rh: 9.1%); IOFF (lh: 0.5%; rh: 3.4%); ILF (rh: 8.4%); CC (body: 18.6%)	3.8	0, -1, 11
<b>DS backward</b>					
FA <sub>T</sub>	Positive	4613	Fornix (body and column: 67.1%) (peak) CC (body: 12.4%; splenium: 14.8%); anterior cingulum (lh: 7.7%; rh: 18.4%); forceps major (3.6%); IOFF (lh: 0.5%; rh: 9.7%); ILF (lh: 2.2%; rh: 4.2%); hippocampal cingulum (lh: 5.5%; rh: 3.2%)	4.58	1, -1, 12
	Positive	215	Posterior corona radiata (lh: 6.4%) (peak) SLF (lh: 9.1%); CC (body: 1.4%); ATR (lh: 7.7%)	3.77	-21, -32, 36
AD <sub>T</sub>	Positive	4622	Fornix (body and column: 61.4%) (peak) CC (splenium: 14.1%); hippocampal cingulum (rh: 4%); ATR (rh: 14.6%); forceps major (15.8%); IOFF (rh: 13.9%); ILF (lh: 0.3%; rh: 6.1%)	4.57	0, -7, 18

ADT = free-water corrected axial diffusivity; ALIC = anterior limb of internal capsule; ANTs = advanced normalization tools; ATR = anterior thalamic radiation; CC = corpus callosum; FAT = free-water corrected fractional anisotropy; ILF = inferior longitudinal fasciculus; IOFF = inferior occipitofrontal fasciculus; lh = left hemisphere; PLIC = posterior limb of internal capsule; rh = right hemisphere; SLF = superior longitudinal fasciculus; UF = uncinat fasciculus. Percentages correspond to % overlap with tracts on the JHU white matter atlas.<sup>30</sup>



**Table 3** Correlations between memory outcome and structural measures

	$\Delta$ FCSRT delayed free recall	$\Delta$ FCSRT total recall	$\Delta$ DS forward	$\Delta$ DS backward
ChBF	0.442**	0.006	0.355*	<b>0.493***</b>
Hippocampal tail	0.374*	0.338*	0.002	−0.008
Subiculum	<b>0.680***</b>	0.269	0.416*	0.426**
CA1	0.138	−0.009	0.272	0.3*
Hippocampal fissure	<b>0.513***</b>	0.382**	0.210	0.151
Presubiculum	−0.096	−0.095	0.045	0.121
Parasubiculum	0.324*	0.395*	0.035	0.002
Molecular layer HP	−0.138	−0.156	−0.058	0.104
GCMLDG	−0.194	−0.139	−0.071	0.091
CA3	−0.269	−0.196	−0.083	0.001
CA4	0.476**	−0.026	0.359*	0.344*
Fimbria	0.035	0.078	−0.204	0.032
HATA	−0.076	0.011	−0.023	0.104
Fornix FA <sub>T</sub>	<b>0.816***</b>	0.424*	0.324*	0.184
Fornix AD <sub>T</sub>	<b>0.748***</b>	0.364*	0.435**	0.474**
Fornix RD <sub>T</sub>	0.433**	0.162	0.268	0.412**
Fornix FW	<b>−0.658***</b>	−0.278*	−0.243	<b>−0.502***</b>

Correlations are adjusted for age and sex, MoCA baseline score and baseline memory performance (corresponding to each difference score). AD<sub>T</sub> = free-water corrected axial diffusivity; CA = cornu ammonis; FA<sub>T</sub> = free-water corrected fractional anisotropy; GCMLDG = granule cell and molecular layers of the dentate gyrus; HATA = hippocampus–amygdala transition area; HP = hippocampus; RD<sub>T</sub> = free-water corrected radial diffusivity. \* $P < 0.05$ , uncorrected; \*\* $P < 0.01$ , uncorrected; \*\*\* $P < 0.001$ , uncorrected; correlations that reached significance controlled for multiple comparisons with a FDR of 5% ( $q < 0.05$ ) are highlighted in italics; correlations that reached significance controlled for multiple comparisons with a FDR of 1% ( $q < 0.01$ ) are highlighted in bold.

association with each of the grey and white matter structural measures.

Analysis based on tractography and tract-specific microstructural measures confirmed an association between fornix microstructure and improvement of both long-term episodic memory and working memory (DS backwards) scores. Improvement in verbal recall performance was also associated with volume of hippocampal subfields (subiculum, hippocampal fissure, hippocampal tail, CA4, parasubiculum) and grey matter volume in the ChBF. Improvement in working memory performance was also positively associated with grey matter volume in hippocampal subfields and ChBF. The pattern of associations was similar for episodic and working memory and changed little when adding risk factors as covariates (Supplementary Table 1).

The anatomical pattern of association between grey matter volume and cognitive change was examined in a voxel-based analysis limited to the ChBF. Associations between grey matter volume and memory outcome were limited to a region that corresponds to the anterior and intermediate nucleus basalis of Meynert (Fig. 4). Here, grey matter volume was positively associated with improvement of both FCSRT delayed free recall [ $F(5,34) = 6.3$ ,  $P = 0.009$ ] and DS backward [ $F(5,36) = 3.71$ ,  $P = 0.047$ ]. After controlling for risk factors, grey matter volume in the nucleus basalis of Meynert remained positively associated with improved FCSRT delayed free recall [ $F(13,26) = 3.63$ ,  $P = 0.048$ ], but only showed a trend-level association with DS backward [ $F(13,28) = 1.85$ ,  $P = 0.087$ ].

## Collective prediction of outcome

SVRs were used to build a model from hippocampal subfields, ChBF volume and fornix measurements in training sets, which were then used to predict memory outcomes in test sets. Evaluation of the distribution of generalization errors across permutations revealed that none of the mean squared error (MSE) values were outliers for linear or Gaussian models (Supplementary Fig. 3). SVR models with a linear kernel performed better for FCSRT delayed free recall ( $MSE_{lin} = 10.4$ ;  $MSE_{gaus} = 12.7$ ), FCSRT total recall ( $MSE_{lin} = 4.3$ ;  $MSE_{gaus} = 5.7$ ) and DS backward ( $MSE_{lin} = 0.8$ ;  $MSE_{gaus} = 1.6$ ). Models with a Gaussian kernel performed better for DS forward ( $MSE_{lin} = 1.7$ ;  $MSE_{gaus} = 0.7$ ). Trained SVR models predicted FCSRT delayed free recall ( $= 0.62$ ,  $P < 0.001$ ) and DS backward ( $= 0.41$ ,  $P < 0.001$ ) in the test sets (Fig. 5). SVR models performed less well in the test sets of FCSRT total recall ( $= 0.02$ ,  $P = 0.08$ ) and DS forward ( $= 0.03$ ,  $P = 0.06$ ). None of the SVR models using lesion characteristics as predictor variables were able to predict memory outcome in the test sets (detailed analyses are provided in the Supplementary material).

## Discussion

The structural status of the fornix, hippocampus and ChBF approximately 3 months after stroke predicted improvement in cognitive performance over the subsequent 9 months. This was true of long-term episodic memory, represented by verbal recall, and working memory, reflected by backwards DS. The anatomical pattern of associations was strikingly similar for recovery in these cognitive domains, despite the segregated anatomy of the networks supporting these functions in the healthy brain. The pattern of associations suggests that the ChBF, hippocampus and fornix are part of a common system that enables recovery across cognitive domains.

The fornix and hippocampus, as part of the extended hippocampal system, play a critical role in recollection in humans.<sup>6,34</sup> The fornix has an intimate anatomical relationship with the hippocampus and particularly the subiculum, with the majority of efferent projections in the fornix arising in this part of the hippocampal formation.<sup>33</sup> This relationship between fornix and subiculum accords with the pattern of results in this study, with associations with improvements in cognitive performance most convincingly demonstrated for the subiculum, and also align with a previous study suggesting that subiculum and fornix are part of a single system implicated in ageing effects on recollection.<sup>35</sup> Damage to the fornix, from tumour, trauma or surgical resection, leads to a major deficit in verbal recall, with relative sparing of familiarity memory.<sup>36,37</sup> A role for the hippocampus in short-term or working memory is more controversial. However, contributions to effective learning strategies in visual memory encoding<sup>38</sup> and short-term visual memory for complex objects<sup>39</sup> have been described and the view that the medial temporal lobe exclusively supports long-term episodic memory challenged.<sup>40</sup> Furthermore, successful working memory performance is dependent on theta neural oscillations derived from the hippocampus.<sup>8</sup> Spatial memory deficits after experimental stroke in rodents also correlate with loss of prefrontal cortex coherence in hippocampally derived theta oscillations<sup>41</sup> and hippocampal inputs play a role in the development of working memory capability and developmental neuroplasticity of regions relevant for working memory such as the dorsolateral prefrontal cortex.<sup>42</sup> The volume of the ChBF showed parallel associations with both working and episodic memory. While the role of the hippocampus in working memory is controversial, the role of the

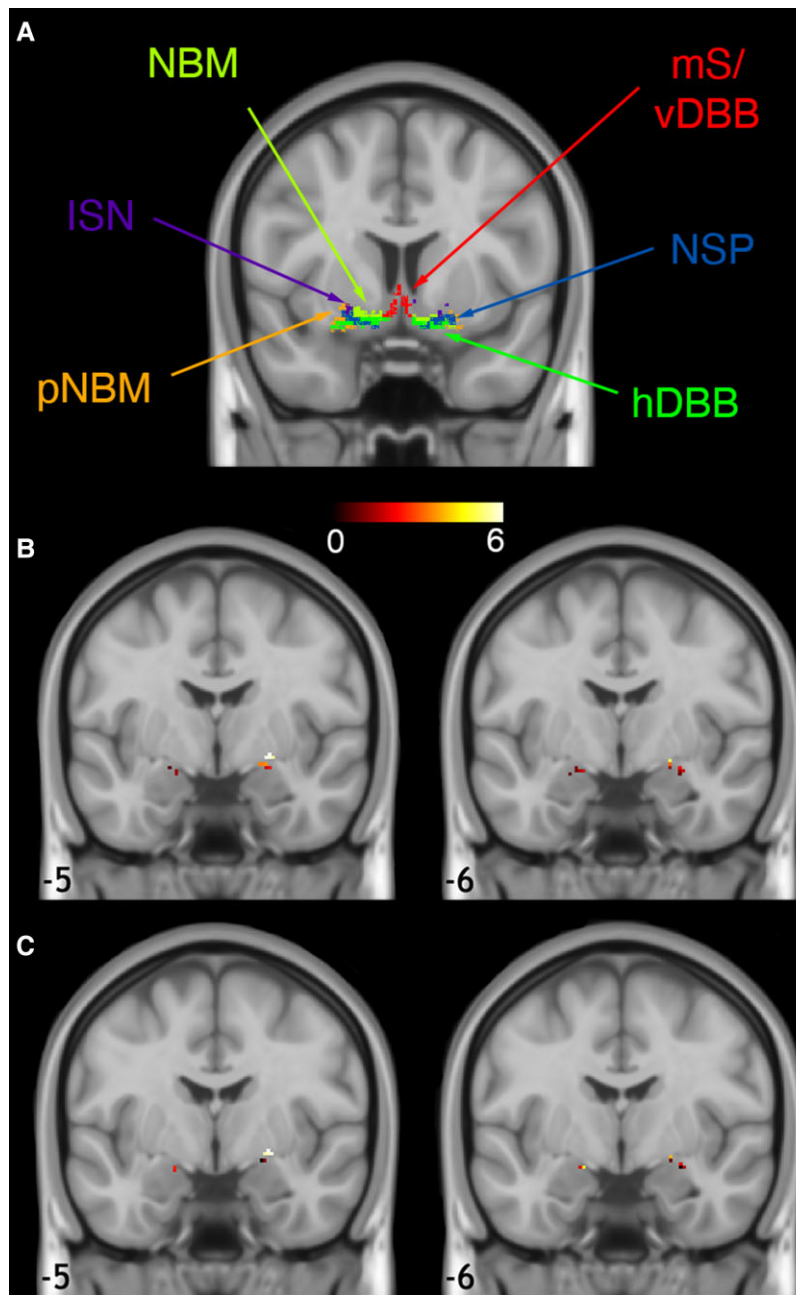


**Figure 4** Voxelwise volumetric evaluation of the ChBF and memory recovery. (A) shows masks of the ChBF as reference. ChBF is displayed at maximum intensity projection for better visibility. hDBB = horizontal limb of the diagonal band of Broca; ISN = interstitial nuclei; mS/vDBB = medial septum and the vertical limb of the diagonal band of Broca; NBM = anterior and intermediate nucleus basalis Meynert; pNBM = posterior nucleus basalis Meynert; NSP = nucleus subputaminalis. Volume in the pNBM was positively associated with memory improvement from 3 to 12 months on (B) FCSRT delayed free recall and (C) DS backward.

cholinergic system in both episodic and working memory is well established. Scopolamine, a cholinergic antagonist, has clear negative effects on performance of both classical working memory<sup>43</sup> and episodic memory tasks.

A critical but sometimes overlooked aspect in explaining the similar pattern of associations for fornix–hippocampus and ChBF is the likely interaction between these two systems. For working memory, a complex interplay between septohippocampal inputs and hippocampal signals is critical to successful memory performance.<sup>8</sup> Lesions limited to the extended hippocampal system have

also been shown to interrupt cholinergic activity within the hippocampus. In this context, it is important to acknowledge that the fornix is a bidirectional pathway for which the hippocampal projections to the mammillary bodies, most implicated in recollection, are only one component. It also contains afferent cholinergic projections to the hippocampal formation (from the vertical limb and the diagonal band of Broca of the basal forebrain) as well as other efferent pathways to ventral striatum, basal forebrain and prefrontal cortex. Experimental lesions in the macaque support the importance of interaction between the cholinergic and

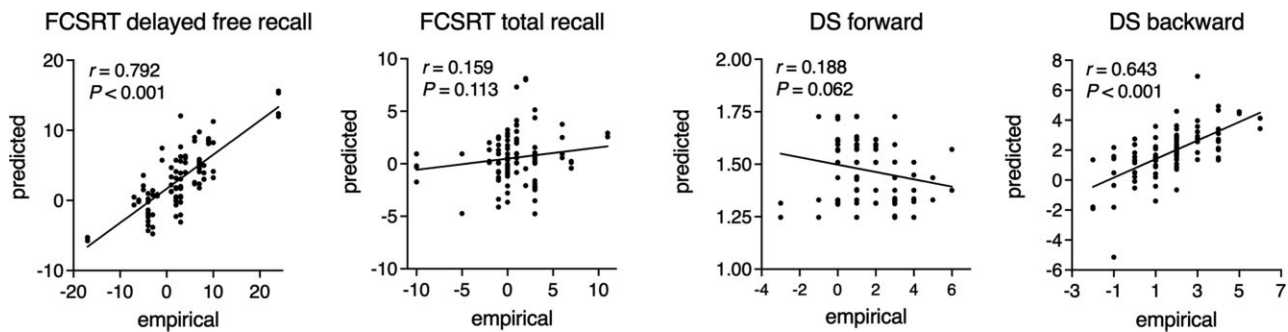


**Figure 5 SVR predictions.** Training sets were used to run four separate SVRs with hippocampal subfields, ChBF volume and fornix measurements as predictor variables, and memory outcomes (FCSRT free recall/FCSRT total recall/DS forward/DS backward) as outcome variables. Cross-validation was performed by testing the regression models derived from the training sets in test sets. Empirical (observed) memory outcome scores on the x-axis are plotted against predicted memory outcome scores on the y-axis.

extended hippocampal systems in adaptation after injury. Cholinergic depletion performed prior to fornix transection produced a more profound learning deficit than when the order of these lesions was reversed.<sup>9</sup> Although the design of the current study does not allow interrogation of the independent roles of these systems, the similar pattern of associations suggests that they are part of a collective infrastructure that supports recovery after injury.

In a recent human imaging study, we found evidence that the cholinergic system supports adaptation to compromise of the fornix through a realignment of cognitive load to alternative white matter pathways.<sup>10</sup> Because human stroke almost inevitably causes injury to white matter pathways, it was hypothesized that the latter mechanism of adaptation would lead to an association between status of the cholinergic system and cognitive recovery. The significant associations between ChBF volumes and change scores for both episodic and working memory support this hypothesis. A voxel-based analysis within the basal forebrain suggested that this association was strongest in parts of the ChBF that correspond with the nucleus basalis of Meynert (Fig. 4). The nucleus basalis provides cholinergic innervation to the neocortex, not the hippocampal formation, which receives cholinergic afferents predominantly from the medial septum and diagonal band of Broca. The results suggest, therefore, that it is the outflow to the neocortex that is important in improvement in cognitive performance after stroke. This pattern of results is therefore consistent with studies showing reorganization of function in the cerebral cortex in conjunction with recovery of language<sup>5</sup> or motor deficits after stroke.

No associations were found between baseline grey matter structure and cognitive change over time. The current study was limited to analysis of baseline structure and subsequent cognitive change. One weakness of the design was that follow-up assessment was not accompanied by repeat imaging. Therefore, the study was sensitive to structural features that would enable subsequent plasticity but not to structural alterations accompanying plasticity. Furthermore, it is not clear whether engagement of multiple-demand cortex to improve performance after injury involves change in cortical structure or simply functional recruitment of cortex. Sensitivity to structural features that enable subsequent plasticity is consistent with the pattern of results: a role of the ChBF in enabling subsequent cortical plasticity is consistent with prior knowledge. The results suggest that the subiculum and fornix are also part of an underlying infrastructure that enables plasticity in the period 3–12 months after injury. Future studies

with detailed imaging at multiple time points will be able to test the prediction that status of a system including ChBF, fornix and hippocampus will predict subsequent grey matter plasticity and functional reorganization. The fornix was the only white matter tract with a majority of fibres (>60% of voxels) were reliably associated with memory outcome across all whole-brain white matter analyses. However, other tracts were implicated with smaller proportional overlaps. These included projection pathways such as the corticospinal tract and anterior thalamic radiation, limbic white matter including the cingulum bundle and uncinate fasciculus, association pathways involved in language, namely the inferior occipito-frontal fasciculus and superior longitudinal fasciculus as well as subsections of the corpus callosum. Future studies may wish to investigate the contribution of these white matter tracts to memory outcome in stroke survivors.

The importance of a common mechanism for cognitive recovery lies in the potential to manipulate and enhance such mechanisms therapeutically. Previous studies examining the relationship between stroke and cholinergic activity showed a decrease in cells and fibres staining positively for key markers of cholinergic activity (choline acetyltransferase and acetylcholinesterase), indicating a cholinergic deficit.<sup>44,45</sup> One drug that has been used to improve cholinergic deficits in Alzheimer’s disease patients is donepezil.<sup>46</sup> Trials of donepezil in stroke patients, however, have not consistently shown efficacy.<sup>47–50</sup> One important potential reason is uncertainty as to the treatment window of donepezil after stroke.<sup>47,48</sup> Another possibility is that enhancement is effective only in individuals with an established cholinergic deficit, so that advanced neuroimaging approaches, as used in this study, could play a role in a personalized medicine approach. Therapeutic stimulation of the fornix has also been proposed as a possible approach to enhance cognition.<sup>51</sup> If the fornix has a broader role in cognitive adaptation and recovery, as the current results suggest, then the possible indications for therapeutic stimulation could extend to enhancing recovery from focal brain injury.

## Acknowledgements

The authors would like to thank Professor John Aggleton, Cardiff, UK and the participants of the 2nd Stroke Recovery and Rehabilitation Roundtable for helpful discussions. We thank the research coordinators of the King’s College Hospital Hyperacute Stroke Research Centre, London, UK, for support with recruitment.

## Funding

This work was supported by the Medical Research Council, UK, grant reference MR/K022113/1 and the European Commission Horizon 2020 CoSTREAM project (grant agreement no. 667375). M.O.S. and L.O. are supported by a strategic award from the Deputy Vice-Chancellor for Research and Innovation, University of Queensland.

## Competing interests

The authors report no competing interests and are aware of no actual, perceived or potential conflicts of interest.

## Supplementary material

[Supplementary material](#) is available at [Brain](#) online.

## References

- Ballard C, Rowan E, Stephens S, Kalaria R, Kenny RA. Prospective follow-up study between 3 and 15 months after stroke: Improvements and decline in cognitive function among dementia-free stroke survivors <75 years of age. *Stroke*. 2003;34:2440–2444.
- Lugtmeijer S, Geerligs L, de Leeuw FE, de Haan EHF, Kessels RPC, Visual Brain G. Are visual working memory and episodic memory distinct processes? Insight from stroke patients by lesion-symptom mapping. *Brain Struct Funct*. 2021;226(6):1713–1726.
- Duncan J. The multiple-demand (MD) system of the primate brain: Mental programs for intelligent behaviour. *Trends Cogn Sci*. 2010;14(4):172–179.
- Shashidhara S, Mitchell DJ, Erez Y, Duncan J. Progressive recruitment of the frontoparietal multiple-demand system with increased task complexity, time pressure, and reward. *J Cogn Neurosci*. 2019;31(11):1617–1630.
- Geranmayeh F, Chau TW, Wise RJS, Leech R, Hampshire A. Domain-general subregions of the medial prefrontal cortex contribute to recovery of language after stroke. *Brain*. 2017;140(7):1947–1958.
- Aggleton JP, Brown MW. Interleaving brain systems for episodic and recognition memory. *Trends Cogn Sci*. 2006;10(10):455–463.
- Rottschy C, Langner R, Dogan I, et al. Modelling neural correlates of working memory: A coordinate-based meta-analysis. *Neuroimage*. 2012;60(1):830–846.
- Zhang Y, Cao L, Varga V, et al. Cholinergic suppression of hippocampal sharp-wave ripples impairs working memory. *Proc Natl Acad Sci U S A*. 2021;118(15):e2016432118.
- Croxson PL, Browning PGF, Gaffan D, Baxter MG. Acetylcholine facilitates recovery of episodic memory after brain damage. *J Neurosci*. 2012;32:13787–13795.
- Ray NJ, Metzler-Baddeley C, Khondoker MR, et al. Cholinergic basal forebrain structure influences the reconfiguration of white matter connections to support residual memory in mild cognitive impairment. *J Neurosci*. 2015;35(2):739–747.
- Conner JM, Chiba AA, Tuszynski MH. The basal forebrain cholinergic system is essential for cortical plasticity and functional recovery following brain injury. *Neuron*. 2005;46(2):173–179.
- Conner JM, Culberson A, Packowski C, Chiba AA, Tuszynski MH. Lesions of the basal forebrain cholinergic system impair task acquisition and abolish cortical plasticity associated with motor skill learning. *Neuron*. 2003;38(5):819–829.
- Teipel SJ, Flatz WH, Heinsen H, et al. Measurement of basal forebrain atrophy in Alzheimer's disease using MRI. *Brain*. 2005;128(11):2626–2644.
- Fazekas F, Kleinert R, Offenbacher H, et al. Pathologic correlates of incidental MRI white matter signal hyperintensities. *Neurology*. 1993;43(9):1683–1689.
- Nasreddine ZS, Phillips NA, Bédirian V, et al. The Montreal Cognitive Assessment, MoCA: A brief screening tool for mild cognitive impairment. *J Am Geriatr Soc*. 2005;53(4):695–699.
- Grober E, Buschke H, Crystal H, Bang S, Dresner R. Screening for dementia by memory testing. *Neurology*. 1988;38(6):900.
- Wambach D, Lamar M, Swenson R, Penney DL, Kaplan E, Libon DJ. Digit span. In: Kreutzer JS, DeLuca J, Caplan B, eds. *Encyclopedia of clinical neuropsychology*. Springer; 2011:844–849.
- Marques JP, Kober T, Krueger G, van der Zwaag W, Van de Moortele P-F, Gruetter R. MP2RAGE, a self bias-field corrected sequence for improved segmentation and T1-mapping at high field. *Neuroimage*. 2010;49(2):1271–1281.
- Ashburner J. A fast diffeomorphic image registration algorithm. *Neuroimage*. 2007;38(1):95–113.
- Leemans A, Jeurissen B, Sijbers J, Jones DK. ExploreDTI: A graphical toolbox for processing, analyzing, and visualizing diffusion MR data. In: 17th Annual Meeting of International Society Magnetic Resonance Medicine. 2009.
- Pasternak O, Sochen N, Gur Y, Intrator N, Assaf Y. Free water elimination and mapping from diffusion MRI. *Magn Reson Med*. 2009;62(3):717–730.
- Jenkinson M, Beckmann CF, Behrens TE, Woolrich MW, Smith SM. FSL. *Neuroimage*. 2012;62(2):782–790.
- Jeurissen B, Leemans A, Jones DK, Tournier JD, Sijbers J. Probabilistic fiber tracking using the residual bootstrap with constrained spherical deconvolution. *Hum Brain Mapp*. 2011;32(3):461–479.
- Tax CM, Jeurissen B, Vos SB, Viergever MA, Leemans A. Recursive calibration of the fiber response function for spherical deconvolution of diffusion MRI data. *Neuroimage*. 2014;86:67–80.
- Tustison NJ, Avants BB, Cook PA, et al. Logical circularity in voxel-based analysis: normalization strategy may induce statistical bias. *Hum Brain Mapp*. 2014;35(3):745–759.
- Klein A, Andersson J, Ardekani BA, et al. Evaluation of 14 non-linear deformation algorithms applied to human brain MRI registration. *Neuroimage*. 2009;46(3):786–802.
- Van Hecke W, Leemans A, Sage CA, et al. The effect of template selection on diffusion tensor voxel-based analysis results. *Neuroimage*. 2011;55(2):566–573.
- Avants BB, Tustison NJ, Song G, Cook PA, Klein A, Gee JC. A reproducible evaluation of ANTs similarity metric performance in brain image registration. *Neuroimage*. 2011;54(3):2033–2044.
- Avants BB, Epstein CL, Grossman M, Gee JC. Symmetric diffeomorphic image registration with cross-correlation: Evaluating automated labeling of elderly and neurodegenerative brain. *Med Image Anal*. 2008;12(1):26–41.
- Mori S, Wakana S, Nagae-Poetscher LM, van Zijl PC. *MRI atlas of human white matter*. Elsevier; 2005.
- Iglesias JE, Augustinack JC, Nguyen K, et al. A computational atlas of the hippocampal formation using ex vivo, ultra-high resolution MRI: Application to adaptive segmentation of in vivo MRI. *Neuroimage*. 2015;115:117–137.
- Desikan RS, Ségonne F, Fischl B, et al. An automated labeling system for subdividing the human cerebral cortex on MRI scans into gyral based regions of interest. *Neuroimage*. 2006;31(3):968–980.
- Saunders RC, Aggleton JP. Origin and topography of fibers contributing to the fornix in macaque monkeys. *Hippocampus*. 2007;17(5):396–411.

34. Aggleton JP. Multiple anatomical systems embedded within the primate medial temporal lobe: Implications for hippocampal function. *Neurosci Biobehav Rev.* 2012;36(7):1579–1596.
35. Hartopp N, Wright P, Ray NJ, et al. A key role for subiculum–fornix connectivity in recollection in older age. *Front Syst Neurosci.* 2018;12:70.
36. Tsivilis D, Vann SD, Denby C, et al. A disproportionate role for the fornix and mammillary bodies in recall versus recognition memory. *Nat Neurosci.* 2008;11(7):834–842.
37. Aggleton JP, McMackin D, Carpenter K, et al. Differential cognitive effects of colloid cysts in the third ventricle that spare or compromise the fornix. *Brain.* 2000;123(Pt 4):800–815.
38. Kragel JE, Schuele S, VanHaerents S, Rosenow JM, Voss JL. Rapid coordination of effective learning by the human hippocampus. *Sci Adv.* 2021;7(25):eabf7144.
39. Koen JD, Borders AA, Petzold MT, Yonelinas AP. Visual short-term memory for high resolution associations is impaired in patients with medial temporal lobe damage. *Hippocampus.* 2017;27(2):184–193.
40. Ranganath C, Blumenfeld RS. Doubts about double dissociations between short- and long-term memory. *Trends Cogn Sci.* 2005;9(8):374–380.
41. Hillman KL, Wall HJ, Matthews LO, Gowing EK, Clarkson AN. Altered hippocampal–prefrontal dynamics following medial prefrontal stroke in mouse. *Neuromolecular Med.* 2019;21(4):401–413.
42. Heuer E, Bachevalier J. Neonatal hippocampal lesions in rhesus macaques alter the monitoring, but not maintenance, of information in working memory. *Behav Neurosci.* 2011;125(6):859–870.
43. Green A, Ellis KA, Ellis J, et al. Muscarinic and nicotinic receptor modulation of object and spatial n-back working memory in humans. *Pharmacol Biochem Behav.* 2005;81(3):575–584.
44. Kataoka K, Hayakawa T, Kuroda R, Yuguchi T, Yamada K. Cholinergic deafferentation after focal cerebral infarct in rats. *Stroke.* 1991;22(10):1291–1296.
45. Sharp SI, Francis PT, Elliott MS, et al. Choline acetyltransferase activity in vascular dementia and stroke. *Dement Geriatr Cogn Disord.* 2009;28(3):233–238.
46. Cacabelos R. Donepezil in Alzheimer's disease: From conventional trials to pharmacogenetics. *Neuropsychiatr Dis Treat.* 2007;3(3):303–333.
47. Barrett KM, Brott TG, Brown RD Jr, et al. Enhancing recovery after acute ischemic stroke with donepezil as an adjuvant therapy to standard medical care: results of a phase IIA clinical trial. *J Stroke Cerebrovasc Dis.* 2011;20(3):177–182.
48. Berthier ML, Pujol J, Gironell A, et al. Beneficial effect of donepezil on sensorimotor function after stroke. *Am J Phys Med Rehabil.* 2003;82(9):725–729.
49. Black S, Roman GC, Geldmacher DS, et al. Efficacy and tolerability of donepezil in vascular dementia: Positive results of a 24-week, multicenter, international, randomized, placebo-controlled clinical trial. *Stroke.* 2003;34(10):2323–2330.
50. Nadeau SE, Behrman AL, Davis SE, et al. Donepezil as an adjuvant to constraint-induced therapy for upper-limb dysfunction after stroke: An exploratory randomized clinical trial. *J Rehabil Res Dev.* 2004;41(4):525–534.
51. Miller JP, Sweet JA, Bailey CM, Munyon CN, Luders HO, Fastenau PS. Visual–spatial memory may be enhanced with theta burst deep brain stimulation of the fornix: A preliminary investigation with four cases. *Brain.* 2015;138:1833–1842.